CARBON 66 (2014) 285–294

Available at www.sciencedirect.com

ScienceDirect

journal homepage: www.elsevier.com/locate/carbon

Hybrid materials of platinum nanoparticles and thiol-functionalized graphene derivatives

Dorothea Marquardt [a], Fabian Beckert [b], Florence Pennetreau [c], Folke Tölle [b], Rolf Mülhaupt [b], Olivier Riant [c], Sophie Hermans [c,*], Juri Barthel [d], Christoph Janiak [a,*]

[a] Institut für Anorganische Chemie und Strukturchemie, Heinrich – Heine Universität Düsseldorf, Universitätsstraße 1, D-40225 Düsseldorf, Germany

[b] Freiburger Matrialforschungszentrum und Institut für Makromolekulare Chemie, Albert–Ludwigs-Universität, 79104 Freiburg, Germany

[c] Institut IMCN – Pôle MOST, Université catholique de Louvain, Bâtiment Lavoisier, Place Louis Pasteur 1, 1348 Louvain-la-Neuve, Belgium

[d] Gemeinschaftslabor für Elektronenmikroskopie RWTH-Aachen, Ernst Ruska-Centrum für Mikroskopie und Spektroskopie mit Elektronen, D-52425 Jülich, Germany

ARTICLE INFO

Article history:
Received 16 May 2013
Accepted 4 September 2013
Available online 12 September 2013

ABSTRACT

Hybrid materials of platinum nanoparticles (Pt-NP) and thiol-functionalized thermally reduced graphite oxide (TRGO-SH), were synthesized by thermal decomposition of the organometallic precursor methylcyclopentadienyl-trimethylplatinum(IV) in dispersions of TRGO-SH in the ionic liquid 1-*n*-butyl-3-methyl-imidazolium tetrafluoroborate under microwave-assisted heating conditions. For the kinetic stabilization of Pt-NPs on TRGO-SH no additional donor ligands were necessary. The ionic liquid acts as separator of the TRGO-SH graphene sheets and as kinetic stabilizing template in the Pt-nanoparticle formation process. Thiol-functionalization of thermally reduced graphite oxide was carried out using three different synthetic procedures: (1) ring opening of propylene sulfide; (2) xanthate grafting and reduction to thiol; (3) reduction, thioesterfication under Mitsunobu conditions and ester hydrolysis. These three different TRGO-SH materials (1), (2) and (3) had different sulfur contents (1.2, 2.5 and 14 wt.%, respectively) and were used as support materials for platinum nanoparticles. The loading of Pt-NPs on TRGO-SH (1), (2) and (3) was 3.2, 3.5 and 8.8 wt.% with particle diameters determined from transmission electron microscopy of (9 ± 4), (2.5 ± 0.9) and (5 ± 2) nm, respectively.

1. Introduction

Covalent modification of graphene allows to introduce a wide range of functional groups and leads to novel functionalized nanostructures and applications, e.g., sustainable catalytic systems, sensing and materials for energy conversion and storage devices [1–4]. The covalent modification of pristine graphene is very difficult. A graphene derivative and precursor for covalent modification is thermally reduced graphite oxide (TRGO). TRGO contains different oxygen groups directly bound to the carbon skeleton of a two-dimensional graphene-derived backbone (Fig. 1) [2].

Chemical modification of TRGO is possible by different reaction types, e.g., electrophilic substitution, nucleophilic substitution, condensation, and addition [6–8]. Covalent functionalization of TRGO prevents agglomeration and can provide stronger bonding to metal nanocrystals by organic linkers. Functional groups on TRGO surfaces can improve

* *Corresponding author.*
E-mail addresses: rolf.muelhaupt@makro.uni-freiburg.de (R. Mülhaupt), Sophie.Hermans@uclouvain.be (S. Hermans), Ju.barthel@fz-juelich.de (J. Barthel), janiak@uni-duesseldorf.de (C. Janiak).
0008-6223/$ - see front matter
http://dx.doi.org/10.1016/j.carbon.2013.09.002

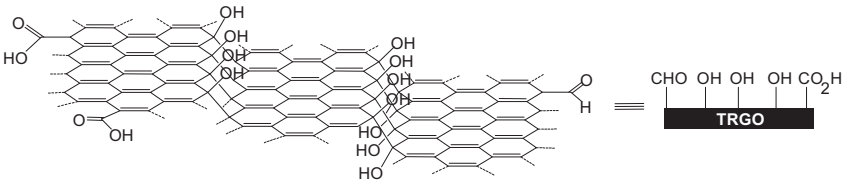

Fig. 1 – Schematic presentation of a model structure for thermally reduced graphite oxide (TRGO) with its functional carboxyl, aldehyde and especially hydroxyl groups according to recent studies [5].

the solubility for solution-phase reactions, for example in the formation of metal-nanoparticle@TRGO hybrid materials [7,8]. Such graphene-supported metal nanoparticle (M-NP) hybrid materials may find applications as chemical sensors [9], as electrodes for fuel cells [10–12], in catalysis [13–16], or for hydrogen storage materials [17]. Metal-nanoparticles on carbon materials are of recent interest for optoelectronics [18–24], and are known for Fe–Co [25], Cu [18], Ag [26,27], Au [19,27], Pt [22,27], Ru [28], or Pd-NPs [28] on exfoliated graphene sheets and other carbon materials. Such hybrid materials were, for example, produced from heating graphite oxide (GO) with the metal complexes $[Pt(NH_3)_4]Cl_2{\cdot}H_2O$, $[Ru(NH_3)_6]Cl_2$ or $[Pd(NH_3)_4]Cl_2{\cdot}H_2O$ under an N_2 atmosphere [28].

Here we report the formation of thiolated graphenes based on TRGO with the aim to improve the immobilization of platinum nanoparticles (Pt-NPs) on such graphene support materials.

2. Experimental section

2.1. Chemicals

LDA (lithium diisopropylamide) and propylene sulfide (2-methylthiirane) were purchased from Sigma Aldrich and used without further purification. Toluene was dried over potassium and freshly distilled prior to use; 1,2 dichloroethane was dried over CaH_2 and distilled under inert atmosphere. Methylcyclopentadienyl-dimer was received from Alfa Aeser, *n*-butyllithium (1.6 mol/L in hexane), methyllithium (1.6 mol/L in diethyl ether) and potassium ethlyl xanthogenate from Sigma Aldrich, potassium iodide 99.5% from Merck, dilauroyl peroxide, hydrazine hydrate (64% hydrazine) and 1,3-dichloroacetone from Acros organics. The ionic liquid 1-*n*-Butyl-3-Methyl-Imidazolium tetrafluoroborate [BMIm][BF_4] was purchased from IoLiTec. The IL was dried and degassed in vacuum (1 h, 85 °C oil bath temperature). (η^5-Methylcyclopentadienyl)trimethylplatinum (IV), (MeCp)$PtMe_3$ was obtained through the reaction of MeCpLi with $(Me_3PtI)_4$ as described elsewhere [38,29,30].

2.2. Instrumentation

Thermal degradation of TRGO-SH was analyzed by means of thermogravimetric analysis with an STA 409 or TG 209 F3 Tarsus (both from Netzsch) at 10 °C/min heating rate using corundum sample holders under nitrogen atmosphere (Figs. S6–S8). The laboratory microwave system was a CEM Discover microwave reactor. Infrared, IR-spectra were measured on a Bruker IR Tensor 37 as KBr pellets. For CHNS elemental analysis an Elementar vario Micro cube instrument was used. Metal analyses were carried out by atom absorption spectroscopy, AAS with a Perkin Elmer AAnalyzer 100. The Pt content was determined from an aqua regia solution of the Pt@TRGO-SH hybrid material. Pt-NP/TRGO-SH samples (minimum amount 3 mg) were digested in hot aqua regia [20 mL, conc. HCl (37%)/conc. HNO_3 (65%) 3:1]. After the aqua regia was boiled down, the residue was re-dissolved in conc. HCl (20 mL, 37%) and boiled down again. The residue was re-dissolved in conc. HCl (37%) and the solution was filtered to remove particles. Aqua regia was added to a total volume of 25 mL followed by AAS analysis.

Powder X-ray diffractograms (PXRD) (example in Fig. S13) were collected with a Bruker D2 Phaser [300 W, 30 kV, 10 mA, Cu-Kα (λ = 1.5406 Å), goniometer radius d = 141 mm], at room temperature using a low-background sample holder without dome. From the platinum metal (1 1 1) reflection the nanocrystal size was calculated according to the Scherrer Eq. (1):

$$\epsilon = \frac{K\lambda}{B\cos\theta_B} \quad (1)$$

with ε = average diameter of nanocrystallites [Å], K = Scherrer factor (0.9) [31]; λ = X-ray wavelength (Cu-K_α = 1.5406 Å), B = half-width of reflection (rad); θ_B = Bragg angle at peak-maximum [31,32].

High resolution transmission electron micrographs (HRTEM) were recorded with a FEI TITAN^3 60–300 electron microscope operated at 80 kV accelerating voltage. The microscope is equipped with a corrector for the chromatic aberration and spherical aberration of the objective and achieves a spatial resolution below 0.1 nm with 80 kV electrons. Particle diameters were manually measured from electron micrographs yielding the medium diameter with standard deviation and diameter distributions in histograms. All samples for HRTEM were prepared by redispersing a small amount of the composite material in acetone under sonication (10 min), placing some of this dispersion on a holey carbon coated copper grid lying on filter paper and drying the grid.

X-ray photoelectron spectroscopy (XPS) analyses were carried out at room temperature on a SSI-X-probe (SSX 100/206) photoelectron spectrometer from Surface Science Instruments (USA) equipped with a monochromatized microfocus Al X-ray source. Graphene samples were stuck on small sample holders with double-face adhesive tape and placed on an insulating ceramic carousel (Macor®, Switzerland). Charge effects were avoided by fixing a nickel grid over the samples and using a 8 eV floodgun. Data were treated with the program CasaXPS (Casa Software Ltd., UK) and the peaks decomposed

into a sum of Gaussian/Lorentzian (85/15) after subtraction of a Shirley type baseline. The energy scale was calibrated with reference to the C1s C-(C,H) peak fixed at 248.8 eV.

^{1}H NMR spectra were recorded on a Bruker spectrometer (300 MHz). Chemical shifts are reported in δ ppm with reference to the residual $CHCl_3$ solvent peak at 7.26 ppm and calibrated to TMS at 0.0 ppm.

High resolution mass spectra (HR-MS) were recorded on a Q-Extractive orbitrap (ThemoFisher). Samples were ionized by atmospheric pressure chemical ionization (APCI) (capillary temperature: 250 °C, vaporizer temperature: 250 °C, sheath gas flow rate: 20 mL/min).

2.3. Synthesis of thermally reduced graphite oxide (TRGO)

Graphite was oxidized to graphite oxide (GO) according to a procedure described by Hummers [33]. This oxidation incorporates functional groups like epoxy and alcohol moieties into the graphite structure. When GO is subjected to rapid heating above 400 °C the functional groups decompose into CO and CO_2 gas which exfoliates the layered GO structure into functionalized thermally reduced graphite oxide (TRGO) sheets [34]. By simply adjusting the reduction temperature, the degree of functionalization can easily be controlled which is a huge benefit of this approach. At a lower reduction temperature more oxygen remains on the TRGO surface and thereby increases the degree of functionalization. This degree of functionalization has a tremendous influence on the dispersibility of TRGO in polar solvents [5]. A higher degree of functionalization improves the dispersibility, e.g., in water or acetone which we ascribe to an increased solvent/solid interaction. For these reasons we reduced GO at 400 °C (hence we also designate the product as TRGO-400) and achieved an oxygen content of 21 wt.% as calculated by the difference to 100% from elemental analysis (77.9% C, 0.7% H). This enabled facile preparation of the TRGO dispersions in ethanol and acetone at concentrations of 1 g/L by means of a high pressure homogenizer (procedure described elsewhere [5]). Briefly this procedure achieved TRGO delamination and deagglomeration by forcing the dispersion through a narrow gap at pressure as high as 1500 bar.

2.4. Reaction of TRGO with propylene sulfide to TRGO-SH(1)

The synthesis of the thiol-functionalized TRGO was carried out according to our recently published procedure [36]. TRGO (2.0 g) was dispersed in toluene (200 mL) by means of high pressure homogenization (1500 bar). LDA (20.0 mL, 1.8 mol) was added at 0 °C. After stirring for 20 min propylene sulfide (7.6 mL, 7.2 g) was added and the mixture was stirred for 1 h at ambient temperature and another 4 h at 65 °C. After filtration and washing with acetone (4 × 200 mL) the product was dried in vacuum (10 mbar, 60 °C).

2.5. Xanthate grafting of TRGO and reduction to TRGO-SH(2) [37]

The *S*-(3-chloro-2-oxopropyl)-*O*-ethyl carbonodithioate compound was synthesized as follows [35]: 4.8 g (30 mmol, 1 equivalent) of potassium ethyl xanthogenate were dissolved in 30 mL of distilled water. The solution was cooled down to 0 °C and 3.8 g (30 mmol, 1 equivalent) of crushed 1,3-dichloroacetone were added in fractions. The solution was stirred for 3 h at 0 °C. The crude mixture was poured in 70 mL of water and 100 mL of diethyl ether. The organic phase was washed with several volumes of water and dried over anhydrous Na_2SO_4. Finally the solvent was removed under reduced pressure to obtain the pure product with yields up to 78%. ^{1}H NMR (300 MHz, $CDCl_3$): δ (ppm) = 1.43 (t, 3H, C**H**$_3$), 4.15 (s, 2H, CO-C**H**$_2$-S), 4.31 (s, 2H, Cl-C**H**$_2$-CO), 4.65 (q, 2H, CH_3-C**H**$_2$-O), HR-MS (APCI): calculated mass for $C_6H_{10}O_2{}^{35}Cl^{32}S_2$ 212.98053 g/mol; measured mass 212.98067 g/mol (see Supporting information).

TRGO (50 mg) was dispersed in a round bottom flask in distilled water (50 mL) and sonicated for 30 min. The suspension was then filtrated (on filters FH, pores 0.5 μm, Millipore) and the solid was washed consecutively with distilled water (100 mL), acetone (100 mL) and diethyl ether (100 mL). The TRGO was finally dried under vacuum for 2 d. At this stage, XPS characterization revealed that, after the washings, only little sulfur (0.02 atom%) is present in the zone corresponding to the xanthate in the XPS spectrum (S analyzed from ~168 eV to ~162 eV). A small amount of chlorine is also found (0.15 atom%) (see Table S1 in Supporting information).

Xanthate grafting proceeded by using *S*-(3-chloro-2-oxopropyl)-*O*-ethyl carbonodithioate as a xanthate carrying a α-chloroketone function and a common radical initiator, dilauroyl peroxide (DLP) in 1,2-dichloroethane (DCE).

Washed TRGO (40.9 mg) was introduced in a three-necked round bottom flask and dried in an oil bath at 100 °C under vacuum overnight. Distilled 1,2-dichloroethane (20 mL) was then added under argon and the slurry was sonicated for 1 h. Subsequently, the dispersion was heated under reflux in a 100 °C oil bath and *S*-(3-chloro-2-oxopropyl)-*O*-ethyl carbonodithioate (724.2 mg) and DLP (136.7 mg) were added with a few milliliters of DCE. After 3 h, DLP (136.2 mg) and a few milliliters of DCE were added and the reaction mixture was heated for an additional 3 h. The crude mixture was then allowed to cool down for 30 min. The dispersion was filtered (on filters GVWP, PVDF, pores 0.22 μm, Millipore) and the solid was washed successively with 100 mL of ethanol, tetrahydrofuran, ethyl acetate and diethyl ether. The modified graphene product was finally suspended in dichloromethane (10 mL) and sonicated for 1 h before being washed as before and dried under vacuum at room temperature overnight.

For the reduction step in order to obtain thiols at the graphene surface, the previously functionalized graphene (14.9 mg) was dispersed in a mixture of absolute ethanol (3 mL) and diethyl ether (2 mL) under argon in a Schlenk tube and was sonicated for 1 h. 1 mL of a solution of hydrazine hydrate (50.6 μL, 64% hydrazine) in diethylether (5 mL) was then added to the dispersion and the resulting mixture was stirred at room temperature for about 70 h. The crude mixture was filtrated (on filters GVWP, PVDF, pores 0.22 μm, Millipore) and washed with ethanol (100 mL), sonicated in acetone for 15 min, washed again with ethanol (150 mL) onto filters FH (pores 0.5 μm, Millipore) and again sonicated in acetone (20 mL) for 15 min. Finally, the solid was washed with diethyl ether (100 mL) and dried under vacuum overnight.

2.6. Reduction of TRGO, Mitsunobu thioesterification and ester hydrolysis to TRGO-SH(3)

TRGO (10 mg) was dispersed in dried THF (10 mL) at 0 °C. $LiAlH_4$ (9.5 mg, 0.25 mmol, 2 eq. relative to 20 wt.% oxygen functionalities on TRGO as calculated from elemental analysis) was added and stirred for 1 h at 0 °C. Afterwards, water (1 mL) was added for quenching. The dispersion was filtered and washed with water (50 mL). The black flaky solid was dried to constant weight at 60 °C.

The product was re-dispersed in THF (10 mL) at 0 °C. Triphenylphosphane, PPh_3 (50 mg, 0.94 mmol, 1.5 eq. referred to TRGO oxygen content) and thioacetic acid (14.2 mg, 13.3 μL, 1.5 eq.) were added and stirred for 5 min. Diisopropyl azodicarboxylate, DIAD (37 mg, 36 μL, 1.5 eq. referred to TRGO oxygen content) was added dropwise and the reaction mixture was allowed to warm up from 0 °C to RT within 12 h. The dispersion was filtered and the residue was washed with water (50 mL). The reaction product was dried to constant weight at 60 °C.

The reaction product was stirred in a solution of potassium hydroxide (35 mg, 0.625 mmol, 5 eq. referred to TRGO oxygen content) in methanol (10 mL) at 0 °C for 30 min. The black reaction product was filtered and the residue was washed with water (30 mL). After the washing the residue was dried at 60 °C to constant weight.

2.7. Pt-NP deposition on thiol-functionalized TRGO, Pt@TRGO-SH hybrid materials (general procedure)

The thiol-functionalized graphene TRGO-SH(1), (2) or (3) (0.1 wt.%, relative to ionic liquid [BMIm][BF_4]) was dispersed in [BMIm][BF_4] under vigorous stirring for 12 h at RT. (MeCp)Pt(Me)$_3$ (9.4 mg, 0.003 mmol, 0.5 wt.% relative to IL) was added under slight warming for emulsification. The reaction mixture was heated under microwave conditions (200 W, run time: 20 s, hold time: 14.5 min) and immediately degassed under reduced pressure to remove volatile byproducts. Water (5 mL) was added to the reaction mixture and the solids separated by centrifugation (15 min, 3500 rpm). The supernatant liquid was decanted and the sediment redispersed in water (8 mL). The dispersion was centrifuged again and the separated liquid phase was removed by decantation. The sediment was dried at 60 °C to constant weight.

3. Results and discussion

3.1. Attempted synthesis of Pt@TRGO

Deposition attempts of Pt-NPs on TRGO-400 have been carried out by dispersing both TRGO-400 (0.2 wt.% relative to IL) and (MeCp)Pt(Me)$_3$ (0.5 wt.%) for 12 h in [BMIm][BF_4] under gentle warming. Then the mixture was heated under microwave conditions (200 W, run time: 20 s, hold time: 14.5 min). Alternatively, the Pt-NP/IL dispersion was prepared first and then the TRGO-400 was stirred in this dispersion for 12 h at room temperature. After work-up as described in Section 2.7 the HRTEM investigations did not show the presence of Pt-NPs on the TRGO-400 flakes (see Fig. 2).

3.2. Thiolation of thermally reduced graphite oxide

The covalent modifications towards thiol-functionalized TRGO were carried out by three different synthetic routes: (1) The hydroxyl functionalities of TRGO were first deprotonated by adding lithium diisopropylamide (LDA) and then reacted with propylene sulfide in toluene to give an S_N^2 ring opening to 1-oxypropane-2-thiol (Fig. 3) [36]. The product TRGO-SH(1) contained about 1.2 wt.% sulfur according to elemental combustion analysis. (2) Xanthate grafting on TRGO was carried out by using S-(3-chloro-2-oxopropyl)-O-ethyl carbonodithioate with the radical initiator dilauroyl peroxide (DLP) in dichloroethane as described recently for carbon nanotubes [37]. X-ray photoelectron spectroscopy (XPS) characterization revealed a much higher concentration in sulfur (0.73%) as well as in chlorine (1.05%), indicating that the xanthate was indeed grafted at the graphene surface (see Table S1 in Supporting information). The grafted xanthate was then

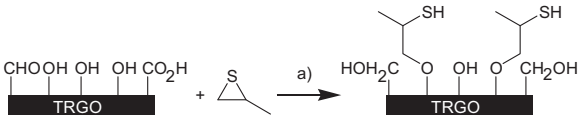

Fig. 3 – Schematic presentation of the ring opening reaction of propylene sulfide (2-methylthiirane) with deprotonated hydroxyl groups of TRGO to yield the material TRGO-SH(1). (a) LDA (lithium diisopropylamide), toluene, 0–65 °C, 5 h.

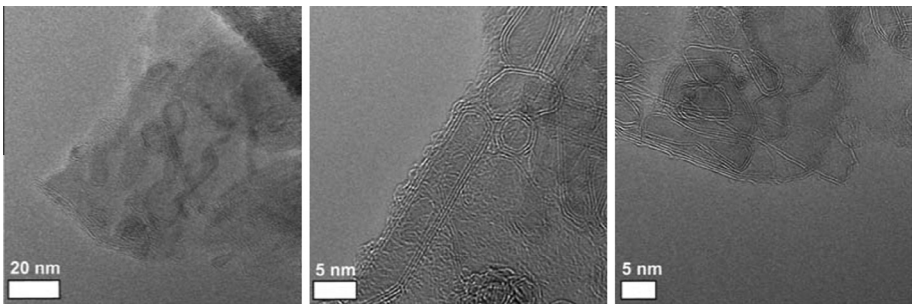

Fig. 2 – HRTEM micrographs from attempted depositions of platinum nanoparticles on non-modified TRGO-400. The micrographs are identical to those of pristine TRGO-400.

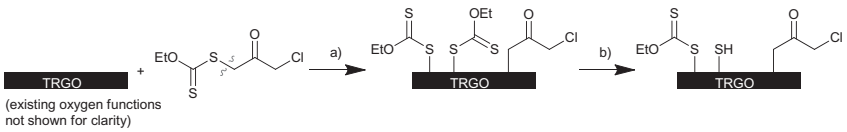

Fig. 4 – Schematic presentation of the xanthate grafting on TRGO to yield the material TRGO-SH(2). (a) DLP (dilauroyl peroxide), 1,2-dichloroethane, 100 °C; (b) $H_2NNH_2{\cdot}H_2O$, EtOH, Et_2O. Note that there is a decrease in Cl content during the reduction step (b) and that the C═O groups on TRGO are also reduced by hydrazine.

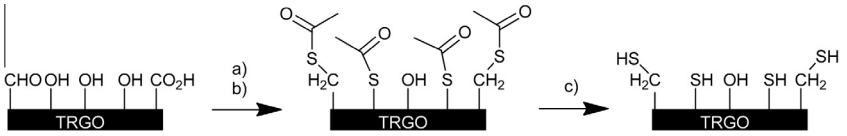

Fig. 5 – Schematic presentation of reduction, Mitsunobu thioesterification and ester hydrolysis of TRGO to yield the material TRGO-SH(3). (a) $LiAlH_4$, THF, 0 °C, 1 h; (b) PPh_3, thioacetic acid, DIAD (diisopropyl azodicarboxylate), THF, 0 °C to RT, 12 h; (c) KOH, MeOH, 0 °C, 30 min.

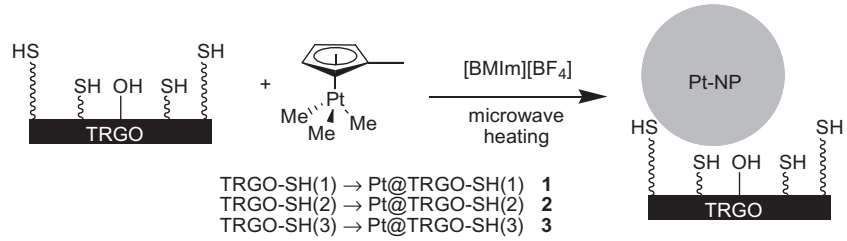

Fig. 6 – Schematic presentation of the formation of Pt@TRGO-SH hybrid materials.

reduced to thiol by hydrazine hydrate (Fig. 4). At this stage, XPS characterization revealed that the peak corresponding to the xanthate effectively decreases; indicating a partial reduction of the xanthate into thiol (Fig. S12 and Table S1). The product TRGO-SH(2) contained about 2.5 wt.% sulfur from combustion elemental analysis. (3) Reduction with $LiAlH_4$, followed by thioesterification under Mitsunobu conditions (PPh_3, thioacetic acid, diisopropyl azodicarboxylate) and ester hydrolysis with KOH (Fig. 5) gave a TRGO-SH(3) material with about 14 wt.% sulfur content.

In the following, the thiol-functionalized graphene is generally abbreviated as TRGO-SH. Designation to the different synthetic procedures and materials is done by the numbers (1)–(3) (cf. Figs. 3–5, respectively). The three thiol-functionalized graphenes TRGO-SH(1–3) are derivatives of thermally reduced graphite oxide (TRGO) and still contain oxygen functionalities (up to 11 atom%) besides the sulfur content according to elemental analysis by X-ray photoelectron spectroscopy for TRGO-SH(2) (Table S1). While TRGO-SH(1) shows a weight loss already starting upon heating at below 100 °C, the TRGO-SH(2) and (3) materials are stable to about 200 °C when a weight loss starts and continues with temperature up to 1000 °C according to thermogravimetric characterization under N_2 atmosphere (Figs. S6–S8).

3.3. *Synthesis of Pt@TRGO-SH hybrid materials*

Platinum nanoparticles (Pt-NP) were synthesized by thermal decomposition of the organometallic precursor methylcyclopentadienyl-trimethylplatinum(IV), $(MeCp)PtMe_3$, as dispersions in ionic liquids (IL) [38]. No additional donor ligands were necessary for the long-time kinetic stabilization of Pt-NPs in imidazolium ionic liquids. Hence, we describe the Pt-NPs in these ILs as "ligand-free" [39]. We note, however, that the exact mechanism of kinetic metal nanoparticle (M-NP) stabilization in ILs is still debated. Small M-NPs appear to be electron deficient or positively charged so that they will be surrounded by oppositely charged ions from ILs in an electrostatic and steric ("electrosteric") stabilizing mechanism [40,41]. Also, metal-N-heterocyclic-carbene and metal-hydride surface species are discussed for M-NP stabilization [42].

In a procedure described previously by us the decomposition of organometallic ruthenium or rhodium carbonyl precursors in dispersions of TRGO in ionic liquids led to formation of M@TRGO hybrid materials [43]. This procedure was not successful for the deposition of Pt-NPs from the $(MeCp)PtMe_3$ precursor. Attempts for the direct use of TRGO as support material with its oxygen donor atoms for Pt-NPs failed. No deposit of Pt-NPs was found by high resolution transmission electron microscopy (HRTEM) on various samples of TRGO which had been in contact with in situ formed Pt-NPs (Fig. 2, left). Also, the particle deposition failed to take place from a pre-formed dispersion of Pt-NP/$[BMIm][BF_4]$ onto the TRGO material at room temperature for 12 h (Fig. 2, middle and right).

Hence, we decided to prepare thiol-functionalized graphene materials to exploit the binding affinity of platinum to sulfur groups. The three different thiol-functionalized

Table 1 – Elemental analysis and platinum nanoparticle diameters of TRGO-SH and Pt@TRGO-SH hybrid materials.

Hybrid	TRGO-SH material	TRGO-SH S; N [wt.%][a]	Pt-NP Ø ± σ [nm][b]	Pt-NP Ø [nm][c]	Pt-Loading [wt.%][a]	Pt@TRGO-SH S; N [wt.%][a]
1	TRGO-SH(1)	1.21; 0.0	9 ± 4	13	3.2	1.24; 3.57
2	TRGO-SH(2)	2.46; 0.0	2.5 ± 0.9	2.5	3.5	0.0; 4.61
3	TRGO-SH(3)	14.26; 0.0	5 ± 2	7	8.8	2.36; 2.90

[a] Elemental analysis. Combustion analysis for sulfur and nitrogen content, atomic absorption spectroscopy for Pt; see Section 2 for details.
[b] Medium diameter Ø and standard deviation σ determined from HRTEM images.
[c] Average diameter calculated from powder X-ray diffraction (PXRD) data using the Scherrer equation.

graphenes TRGO-SH(1)–(3) were tested as support materials for Pt-NPs. In a typical procedure, the thiol-functionalized graphenes TRGO-SH(1)–(3) were dispersed in the ionic liquid 1-*n*-butyl-3-methyl-imidazolium tetrafluoroborate, [BMIm][BF_4] under vigorous stirring in order to exfoliate and separate the graphene sheets. Exfoliation of the graphene sheets should increase the surface area and accessibility for deposition of Pt-NPs. The Pt-NPs are then formed under microwave-assisted thermal decomposition of the Pt-precursor in the TRGO-SH/IL dispersion (Fig. 6).

Ionic liquids are an especially attractive medium for microwave reactions. They efficiently absorb microwave energy due to their ionic character with high polarity, high polarizability and high dielectric constant. Consequently ILs show a high dissipation factor (tan δ) for the conversion of microwave energy into heat [44,45]. Microwaves are a low-frequency energy source which can be used for many chemical reactions [44,46–48]. Microwave radiation directly heats the reaction mixture and not the vessel, i.e., it is the reaction mixture which absorbs the microwave energy. This leads to very fast and efficient heating times up to temperatures of 200 °C within seconds [46,49–51]. Carbon materials are also very sensitive to microwave heating. As soon as metal particles have formed from the decomposition of the precursor, they can also absorb the microwave radiation. Theoretical calculations indicate that due to their high surface-to-volume ratio nanoscopic (metallic or magnetic) particles quickly reach a thermal stationary state upon electromagnetic excitation with negligible temperature difference between the volume phase of the particle and its surrounding. Depending on particle size and surrounding medium initiation times around 100 ps are expected [52–54]. Experimental findings suggests further that the energy transfer between particle and the surrounding phase leads to increased excitation of vibrational degrees of freedom in surface-bound or surface-near molecules which can in turn be used for the activation of reactions.

Thermal decomposition of the metal organic Pt-precursor released volatile fragments of the organic ligands, which can be removed from the reaction mixture under reduced pressure to give ligand-free Pt-NPs with little contamination [55–58]. The Pt-NPs should then attach to the thiol groups on the graphene surface and/or use the –SH functions as nucleation centers.

After reaction the IL was removed by washing with water to isolate the Pt@TRGO-SH hybrid materials. The addition of water to the reaction mixture decreased the viscosity of the dispersion, and it was possible to separate the precipitate by centrifugation. The sediment was carefully washed with water to remove adhered IL as much as possible. Drying in air yielded a solid fluffy powder of dry appearance. After the washing and drying procedure, IR-spectroscopy still showed the B–F stretching vibration between 1000 and 1100 cm^{-1}, which is attributed to the BF_4^- anion of the IL (Figs. S1–S5). Furthermore, elemental nitrogen analyses of the Pt@TRGO-SH materials revealed up to 4.6 wt.% of nitrogen originating from the imidazolium cation of the IL (Table 1). This result indicates that the IL is still part of the Pt-NP@TRGO-SH materials and may be adsorbed as a surface layer of the Pt-NPs and/or the graphene layers or in mesopores formed by the TRGO material. A recent study proposed that ILs can work as nanoglue for sticking Pt nanoparticles against single-walled carbon nanotubes [59].

Thermal stress (microwave heating) of the TRGO-SH material during the Pt-NP formation and deposition process can also lead to loss of sulfur groups. Elemental analysis of the Pt-NP@TRGO-SH composites indicated a decrease of sulfur content in TRGO-SH(2) and (3) (Table 1, hybrid **2** and **3**) from 2.5 to 0 wt.% and from 14 to 2.4 wt.%, respectively. The hybrid material **1** fully kept its sulfur content during the Pt-NP deposition process.

Thiol groups with direct covalent bonding of the sulfur atom to the graphene carbon backbone as in TRGO-SH(2) and (3) apparently suffered from thermal instability during the high-temperature microwave heating procedure for the Pt-loading. Perhaps this sulfur loss can be correlated to the direct heating of the carbon backbone under microwave irradiation. As a result the sulfur content was strongly decreased in hybrid **2** and considerably lowered in hybrid **3**. Note that in TRGO-SH(3) some thiol groups are presumably bound through a methylene spacer to the TRGO net. Even short alkyl spacers apparently contribute to the sulfur group stability during thermal treatment. Still, both in hybrid **2** and **3** Pt-NPs were found on the TRGO surface which were stable under the electron beam in HRTEM.

Platinum nanoparticles were observed for all three Pt@TRGO-SH samples by high-resolution transmission electron microscopy (HRTEM). The graphene sheets of samples Pt@TRGO-SH(1–3) are all decorated with Pt-NPs which clearly separate with dark contrast against the surrounding support material in the images of Figs. 7–9. Only the hybrid **1** from TRGO-SH(1) shows the typical wrinkled structure of thin graphene sheets. The graphene sheets of the hybrids **2** and **3** appear to be thicker and less wrinkled showing a higher contrast. In the TEM images, the material surrounding the Pt-NPs exhibits a partially layered and partially amorphous structure, which may occur due to a projection overlap of randomly oriented small graphene flakes.

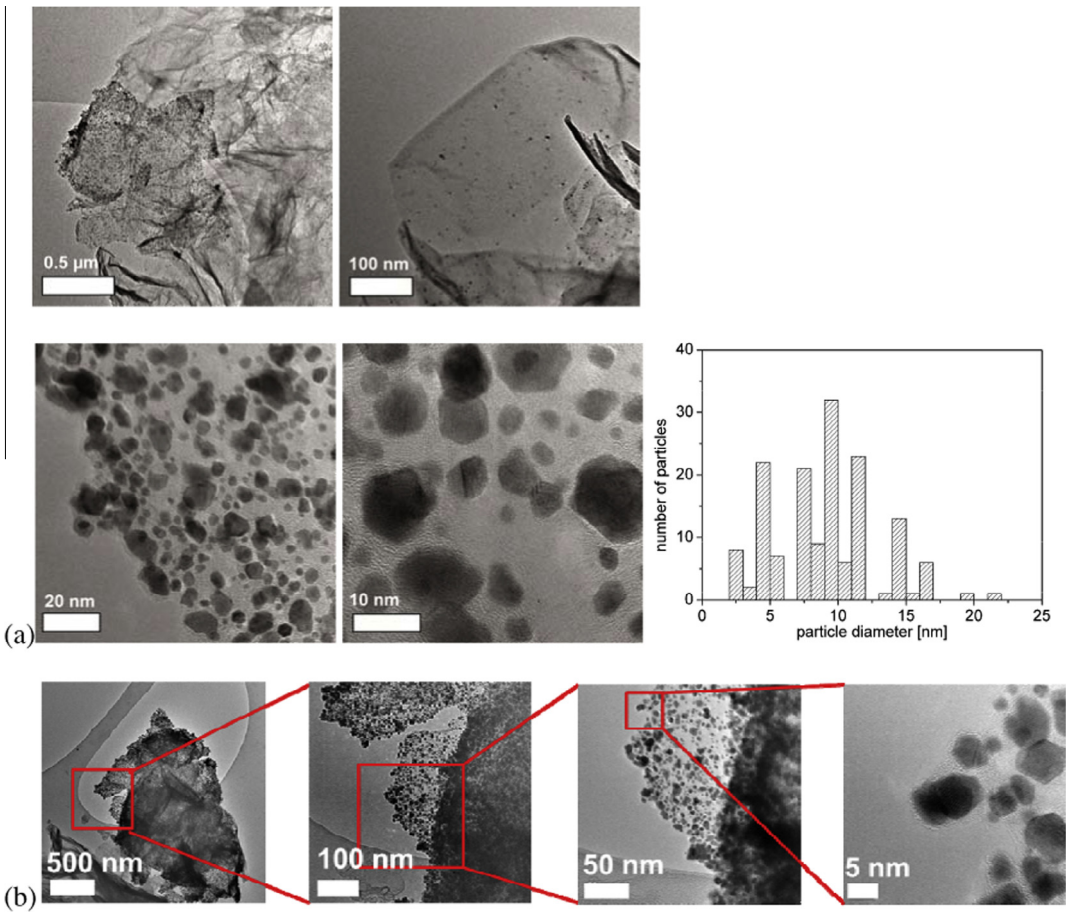

Fig. 7 – (a) HRTEM micrographs of hybrid 1 showing a partly Pt-NP loaded TRGO-SH flake; histogram of particle diameters determined from HRTEM micrographs (150 particles analyzed); (b) sequence of magnification of HRTEM micrograph of hybrid 1.

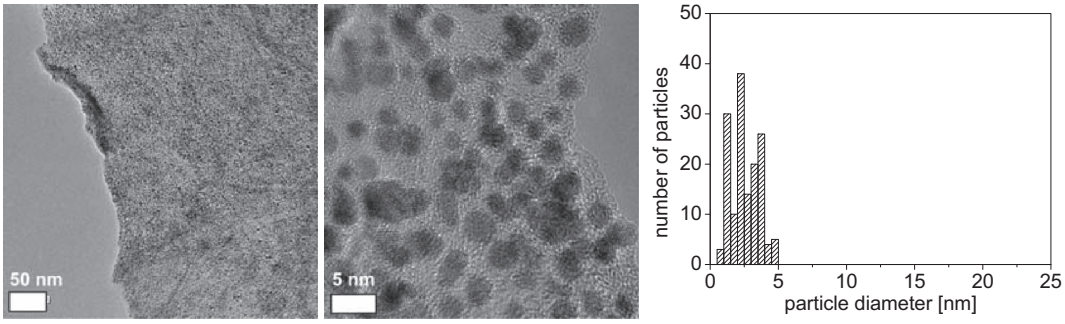

Fig. 8 – HRTEM micrographs of hybrid 2, histogram of particle diameters determined from HRTEM micrographs (150 particles analyzed).

For hybrid **1** Pt-NP particle diameters of (9 ± 4) nm (Table 1) were measured from HRTEM images (Fig. 7). During the electron microscopy process the surface atoms of the platinum particles were seen moving. Larger particles were irregularly shaped. The average diameter of Pt nanocrystals in hybrid **1** was also calculated as 13 nm from PXRD data using the Scherrer equation (see Section 2) with the platinum (111) reflection.

It is noteworthy that some graphene sheets or parts of them were preferred for the deposition of the nanoparticles (Fig. 7a). This can be an artifact of the degree of exfoliation of multi-layered sheets in dispersions: for sulfur functionalization in case (1), only the oxygen functionalities of exposed surfaces from exfoliated sheets are available and can be modified. The nanoparticle formation and deposition procedure in dispersions of IL leads to further mechanical exfoliation of sheets, which were not exposed in the sulfur functionalization process. Pt-NPs most likely prefer to coordinate to the TRGO material through thiol functionalities. Hence, the par-

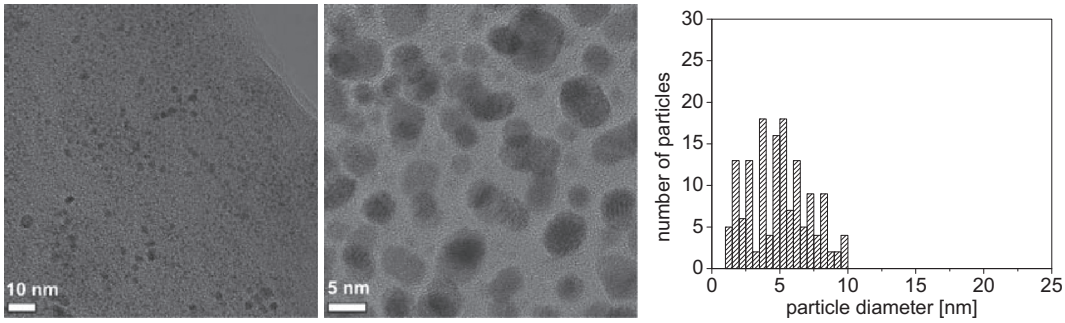

Fig. 9 – HRTEM micrographs of hybrid 3; histogram of particle diameters determined from HRTEM micrographs (150 particles analyzed).

tial Pt-NP deposition on the graphene sheets could be an indirect visualization of sulfur rich regions.

The HRTEM images show that some of the bigger platinum particles on TRGO-SH(1) exhibit defects of the crystal structure which could be interpreted as grain boundaries whereas Pt-NPs on TRGO-SH(2) and (3) appear single crystalline. Bigger particles are very often polycrystalline, while smaller NPs are often single-domain. Hybrid **1** contains the largest particles (up to 20 nm) among the three hybrids (see also below). These larger particles can form by aggregation of smaller particles and can therefore exhibit grain boundaries.

For the hybrid materials **2** and **3** no significant movement of the Pt-NPs on the support was observed during the electron microscopy, which indicates that a complete immobilization of the metal nanoparticles on TRGO-SH was achieved. The Pt-NPs are small and homogenously-shaped with narrow size distributions of (2.5 ± 0.9) nm for hybrid **2** (Fig. 8) and (5 ± 2) nm for hybrid **3** (Fig. 9) as measured from HRTEM images, in good agreement with the diameters of 2.5 nm and 7 nm, as determined by the Scherrer equation (Eq. (1), Table 1). We note that the size distribution of the Pt-NPs in the three different hybrid materials is 2–20 nm for hybrid **1**, 1–5 nm for hybrid **2**, and 1–10 nm for hybrid **3** when taking the average diameter ± 2σ range (see Table 1). The differences in diameters are considerably larger than observed for platinum nanocrystals with small average diameters between 1.0(3) and 2.3(7) nm which were prepared without any additional stabilizers in glycol, glycerol, the ionic liquids (ILs) 1-*n*-butyl-3-methyl-imidazolium tetrafluoroborate [BMIm][BF_4] and *N*-butyl-*N*-trimethyl-ammonium bis(trifluoromethylsulfonyl)amide [N_{4111}][NTf_2] or diphenylmethane (CH_2Ph_2) by thermal, photolytic or microwave assisted decomposition of the organometallic precursor methylcyclopentadienyl-trimethylplatinum(IV), (MeCp)$PtMe_3$ [38]. We have to state that we do not have a proper explanation for this observation yet and want to prevent speculations on this aspect.

The Pt content in the hybrid materials was determined from aqua regia solution by AAS for hybrid **1** to 3.2 wt.%, for hybrid **2** to 3.5 wt.%, and for hybrid **3** to 8.8 wt.%. A trend, but no direct correlation between the sulfur content and the Pt-loading can be deduced.

Among other catalytic reactions, hydrosilylation reaction that are essential in industrial processes are catalyzed by Pt and its alloys [60–64]. The solid Pt@TRGO-SH(1) material was tested as catalyst for the reaction of phenylacetylene with triethylsilane (Fig. S13, see Supporting information for details). These substrates were chosen as a model system for the hydrosilylation of terminal acetylenes with alkylsilanes based on previous studies [38]. The catalytic reaction was carried out under MW conditions as a time and energy saving alternative to the conventional oil bath heating. Compared with previous studies of Pt/[BMIm][BF_4] catalyst dispersions, the solid Pt@TRGO-SH(1) catalyst yielded a low conversion (23%) where under similar conditions with Pt/[BMIm][BF_4] quantitative conversion was reached [38].

4. Conclusions

Hybrid materials Pt@TRGO-SH have been formed under microwave conditions from thiol-functionalized TRGO materials and (MeCp)$PtMe_3$ in the ionic liquid [BMIm][BF_4].

In hybrid **1** the TRGO-SH(1) functionalized graphene material carried 1-oxypropane-2-thiol groups bound to the carbon net. The Pt-NP hybrid formed with TRGO-SH(1) showed the best thermal stability and kept the full sulfur content in the high-temperature Pt-loading process. Whereas the sulfur content in TRGO-SH(2) and (3) was substantially decreased, presumably due to thermal instability of thiol groups which are directly covalently bound to the graphene backbone. Yet, all three TRGO-SH materials formed hybrid material with platinum nanoparticles. The Pt@TRGO-SH(1) flakes exhibit a thin-layered wrinkled structure similar to exfoliated TRGO. The absence of such wrinkles in Pt@TRGO-SH(2) and (3) indicated multi-layered graphene sheets.

In summary, sulfur moieties in functionalized graphene assist the deposition of Pt-NPs through a possible dual role of anchor groups and nucleation centers. This could be advantageously employed in the preparation of platinum-on-carbon electrodes, e.g., for fuel cells.

Appendix A. Supplementary data

Supplementary data associated with this article can be found, in the online version, at http://dx.doi.org/10.1016/j.carbon.2013.09.002.

REFERENCES

[1] You JM, Kim D, Jeon S. Electrocatalytic reduction of H_2O_2 by Pt nanoparticles covalently bonded to thiolated carbon nanostructures. Electrochim Acta 2012;83:288–93.
[2] Dai L. Functionalization of graphene for efficient energy conversion and storage. Acc Chem Res 2013;46:31–42.
[3] Su C, Loh KP. Carbocatalysts: graphene oxide and its derivatives. Acc Chem Res 2013. http://dx.doi.org/10.1021/ar300118v.
[4] He D, Chen K, Li H, Peng T, Xu F, Mu S, et al. Highly active platinum nanoparticles on graphene nanosheets with a significant improvement in stability and CO tolerance. Langmuir 2012;28:3979–86.
[5] Tölle FJ, Fabritius M, Mülhaupt R. Emulsifier-free graphene dispersions with high graphene content for printed electronics and freestanding graphene films. Adv Funct Mater 2012;22:1136–44.
[6] Song M, Xu J, Wu C. The effect of surface functionalization on the immobilization of gold nanoparticles on graphene sheets. J Nanotechnol 2012:5. http://dx.doi.org/10.1155/2012/329318 [Article ID 329318].
[7] Kuila T, Bose S, Mishra AK, Khanra P, Kim NH, Lee HJ. Chemical functionalization of graphene and its applications. Prog Mater Sci 2012;57:1061–105.
[8] Ding M, Tang Y, Star A. Understanding interfaces in metal-graphitic hybrid nanostructures. Phys Chem Lett 2013;4:147–60.
[9] Bui MPN, Lee S, Han KN, Pham XH, Li CA, Choo J, et al. Electrochemical patterning of gold nanoparticles on transparent single-walled carbon nanotube films. Chem Commun 2009;37:5549–51.
[10] Li WZ, Waje M, Chen ZW, Larsen P, Yan YS. Platinum nanoparticles supported on stacked-cup carbon nanofibers as electrocatalysts for proton exchange membrane fuel cell. Carbon 2010;48:995–1003.
[11] Lee G, Shim JH, Kang H, Nam KM, Song H, Park JT. Monodisperse Pt and PtRu/C-60 hybrid nanoparticles for fuel cell anode catalysts. Chem Commun 2009:5036–8.
[12] Seger B, Kamat PV. Electrocatalytically active graphene-platinum nanocomposites. Role of 2-D carbon support in PEM fuel cells. J Phys Chem 2009;113:7990–5.
[13] Dong L, Gari RRS, Li Z, Craig MM, Hou S. Graphene-supported platinum and platinum-ruthenium nanoparticles with high electrocatalytic activity for methanol and ethanol oxidation. Carbon 2010;48:781–7.
[14] Karimi B, Kabiri Esfahani F. Gold nanoparticles supported on Cs_2CO_3 as recyclable catalyst system for selective aerobic oxidation of alcohols at room temperature. Chem Commun 2009:5555–7.
[15] Sun M, Zhang J, Zhang Q, Wang Y, Wan H. Polyoxometalate-supported Pd nanoparticles as efficient catalysts for the direct synthesis of hydrogen peroxide in the absence of acid or halide promoters. Chem Commun 2009:5174–6.
[16] Armelao L, Dell'Amico DB, Braglia R, Calderazzo F, Garbassi F, Marra G, et al. Loading silica with metals (palladium or platinum) under mild conditions by using well-defined molecular precursors. Dalton Trans 2009:5559–68.
[17] Lightcap IV, Kosel TH, Kamat PV. Anchoring semiconductor and metal nanoparticles on a two-dimensional catalyst material. Storing and shuttling electrons with reduced graphene oxide. Nano Lett 2010;10:577–83.
[18] Li HB, Kang WJ, Xi BJ, Yan Y, Bi HY, Zhu YC, et al. Thermal synthesis of Cu@carbon spherical core-shell structures from carbonaceous matrices containing embedded copper particles. Carbon 2010;48:464–9.
[19] Park H, Kim JS, Choi BG, Jo SM, Kim DY, Hong WH, et al. Sonochemical hybridization of carbon nanotubes with gold nanoparticles for the production of flexible transparent conducing films. Carbon 2010;48:1325–30.
[20] Ventura DN, Stone RA, Chen KS, Hariri HH, Riddle KA, Fellers TJ, et al. Assembly of cross-linked multi-walled carbon nanotube mats. Carbon 2012;50:987–94.
[21] Kudo S, Maki T, Miura K, Mae K. High porous carbon with Cu/ZnO nanoparticles made by the pyrolysis of carbon material as a catalyst for steam reforming of methanol and dimethyl ether. Carbon 2010;48:1186–95.
[22] Scholz K, Scholz J, McQuillan AJ, Wagner G, Klepel O. Partially embedded highly dispersed Pt nanoparticles in mesoporous carbon with enhanced leaching stability. Carbon 2010;48:1788–98.
[23] Kim YH, Kim YT, Kim SH, Lee D. Catalytic oxidation kinetics of iron-containing carbon particles generated by spraying ferrocene-mixed with diesel fuel into a hydrogen-air diffusion flame. Carbon 2010;48:2072–84.
[24] Tzitzios V, Georgakilas V, Oikonomou E, Karakassides M, Petridis D. Synthesis and characterization of carbon nanotube/metal nanoparticle composites well dispersed in organic media. Carbon 2006;44:848–53.
[25] Vidick D, Herlitschke M, Poleunis C, Delcorte A, Hermann RP, Devillers M, et al. Comparison of functionalized carbon nanofibers and multi-walled carbon nanotubes as supports for Fe-Co nanoparticles. J Mater Chem A 2013;1:2050–63.
[26] lI j, Liu CY, Kim SH, Lee D. Ag/graphene heterostructures: synthesis, characterization and optical properties. Eur J Inorg Chem 2010:1244–8.
[27] Subrahmanyam KS, Manna AK, Pati SK, Rao CNR. A study of graphene decorated with metal nanoparticles. Chem Phys Lett 2010;497:70–5.
[28] Gotoh K, Kawabata K, Fujii E, Morishige K, Kinumoto T, Miyazaki Y, et al. The use of graphite oxide to produce mesoporous carbon supporting Pt, Ru, or Pd nanoparticles. Carbon 2009;47:2120–4.
[29] Meiere SH, Hoover CA. Methods for producing organometallic compounds. US patent 2004/0010158 A1; 2004.
[30] Meiere SH, Hoover CA, Methods for producing organometallic compounds. US patent 6,809,212 B2; 2006.
[31] Langford JI, Wilson AJC. Scherrer after sixty years: a survey and some new results in the determination of crystallite size. J Appl Cryst 1978;11:102–13.
[32] Crespilho FN, Huguenin NF, Zucolotto V, Olivi P, Nart FC, Oliveira ON. Dendrimers as nanoreactors to produce platinum nanoparticles embedded in layer-by-layer films for methanol-tolerant cathodes. Electrochem Commun 2006;8:348–52.
[33] Hummers WS, Offeman RE. Preparation of graphitic oxide. J Am Chem Soc 1958;80:1339.
[34] Dreyer DR, Park S, Bielawski CW, Ruoff RS. The chemistry of graphene oxide. Chem Soc Rev 2010;39:228–40.
[35] Bergeot O, Corsi C, El Qacemi M, Zard SZ. S-(3-Chloro-2-oxo-propyl)-O-ethyl xanthate: a linchpin radical coupling agent for the synthesis of heterocyclic and polycyclic compounds. Org Biomol Chem 2006;4:278–90.
[36] Beckert F, Friedrich C, Thomann R, Mülhaupt R. Sulfur-functionalized graphenes as macro-chain-transfer and RAFT agents for producing graphene polymer brushes and polystyrene nanocomposites. Macromolecules 2012;45:7083–90.
[37] Vanhorenbeke B, Vriamont C, Pennetreau F, Devillers M, Riant O, Hermans S. Radical addition of xanthates on carbon nanotubes as an efficient covalent functionalization method. Chem Eur J 2013;19:852–6.
[38] Marquardt D, Barthel J, Braun M, Ganter C, Janiak C. Weakly-coordinated stable platinum nanocrystals. CrystEngComm 2012;14:7607–15.

[39] Vollmer C, Janiak C. Naked metal nanoparticles from metal carbonyls in ionic liquids: Easy synthesis and stabilization. Coord Chem Rev 2011;255:2039–57.
[40] Boennemann H, Richards RM. Nanoscopic metal particles – synthetic methods and potential applications. Eur J Inorg Chem 2000:2455–80.
[41] Dupont J, Scholten JD. On the structural and surface properties of transition-metal nanoparticles in ionic liquids. Chem Soc Rev 2010;39:1780–804.
[42] Scholten JD, Leal BC, Dupont J. Transition metal nanoparticle catalysis in ionic liquids. ACS Catal 2012;2:184–200.
[43] Marquardt D, Vollmer D, Thomann R, Steurer P, Mülhaupt R, Redel E, et al. The use of microwave irradiation for the easy synthesis of graphene-supported transition metal nanoparticles in ionic liquids. Carbon 2011;49:1326–32.
[44] Wasserscheid P, Keim W. Ionic liquids – new "solutions" for transition metal catalysis. Angew Chem Int Ed 2000;39:3772–89.
[45] Larhed M, Moberg C, Hallberg A. Microwave-accelerated homogeneous catalysis in organic chemistry. Acc Chem Res 2002;35:717–27.
[46] Bogdal D. Microwave-Assisted Organic Synthesis. New York: Elsevier; 1993. 47–189.
[47] Mingos DMP, Baghurst DR. Applications of microwave dielectric heating effects to synthetic problems in chemistry. Chem Soc Rev 1991;20:1–47.
[48] Galema SA. Microwave chemistry. Chem Soc Rev 1997;26:233–8.
[49] Buchachenko AL, Frankevich EL. Chemical generation and reception of radio- and microwaves. Weinheim: Wiley-VCH; 1993. 41–56.
[50] Ahluwulia VK. Alternative energy processes in chemical synthesis. Oxford: Alpha Science International LTD; 2008.
[51] Bilecka I, Niederberger M. Microwave chemistry for inorganic nanomaterials synthesis. Nanoscale 2010;2:1358–74.
[52] Ahmadi TS, Logunov SL, Elsayed MA. Picosecond dynamics of colloidal gold nanoparticles. J Phys Chem 1996;100:8053–6.
[53] Perner M, Bost P, Lemmer U, von Plessen G, Feldmann J, Becker U, et al. Optically induced damping of the surface plasmon resonance in gold colloids. Phys Rev Lett 1997;78:2192–5.
[54] Andra W, D'Ambly C, Hergt R. Temperature distribution as function of time around a small spherical heat source of local magnetic hyperthermia. J Magn Magn Mater 1999;194:197–203.
[55] Gutel T, Garcia-Antõn J, Pelzer K, Philippot K, Santini CC, Chauvin Y, et al. Influence of the self-organization of ionic liquids on the size of ruthenium nanoparticles: effect of the temperature and stirring. J Mater Chem 2007;17:3290–2.
[56] Chaudret B, Phillipot K. Organometallic nanoparticles of metals or metal oxides. Oil Gas Sci Technol 2007;62:799–817.
[57] Ciuculescu D, Dumestre F, Comensaña-Hermo M, Chaudret B. Single-crystalline Co nanowires: synthesis, thermal stability, and carbon coating. Chem Mater 2009;21:3987–95.
[58] Pagès C, Coppel Y, Kahn ML, Maissonat A, Chaudret B. Self-assembly of ZnO nanocrystals in colloidal solution. ChemPhysChem 2009;10:2334–44.
[59] Yoshii K, Tsuda T, Arimura T, Imanishi A, Torimoto T, Kuwabata S. Platinum nanoparticle immobilization onto carbon nanotubes using Pt-sputtered room-temperature ionic liquid. RSC Adv 2012;2:8262–4.
[60] Troegel D, Stohrer J. Recent advances and actual challenges in late transition metal catalyzed hydrosilylation of olefins from an industrial point of view. Coord Chem Rev 2011;255:1440–50.
[61] Alonso F, Buitrago R, Moglie Y, Ruiz-Martínez J, Sepúlveda-Escribano A, Yus M. Hydrosilylation of alkynes catalysed by platinum on titania. J Organomet Chem 2011;696:368–72.
[62] Jakubek V, Lees AJ. Quantitative photochemistry of $Cp'Pt(CH_3)_3$ ($Cp' = \eta^5$-$C_5H_4CH_3$) in solution: a highly efficient organometallic photoinitiator for hydrosilylation. Inorg Chem 2004;43:6869–71.
[63] Boardman LD. (η^5-Cyclopentadienyl)trialkylplatinum photohydrosilylation catalysts. Mechanism of active catalyst formation and preparation of a novel Bis(sily1)platinum hydride. Organometallics 1992;11:4194–201.
[64] Pârvulescu VI, Hardacre C. Catalysis in ionic liquids. Chem Rev 2007;107:2615–65.